Figure legends

Fig.1 A. C-terminal ghrelin-like immunoreactivity in adult mouse islet. The staining was observed in the peripheral region of the islet. B. Glucagon-like immunoreactivity in serial section.

Fig.2 A: Structure of RIP-ghrelin transgene. B: Structure of RGP-ghrelin transgene. C, D: Pancreatic islet of RIP-ghrelin transgenic mouse stained with anti-ghrelin [13-28] (C) and anti-ghrelin [1-11] antisera (D). E, F: Pancreatic islet of RGP-ghrelin transgenic mouse stained with anti-ghrelin [13-28] (E) and anti-ghrelin [1-11] antisera (F). G: Plasma ghrelin levels collected from retroorbital and portal veins in RIP-G Tg. *: $P<0.05$ compared to retroorbital vein. #: $P<0.01$ compared to nontransgenic littermates. H: The step-up of ghrelin concentration from retroorbital vein to portal vein in RIP-G Tg. #: $P<0.01$ compared to their nontransgenic littermates.

Fig.3 A: Body weight of RIP-G Tg (Tg) and their nontransgenic littermates (non). B: Food intake of RIP-Tg (Tg) and their nontransgenic littermates (non).

Fig. 4 A, B. Blood glucose levels after overnight fast in RIP-G Tg (A) and RGP-G Tg (B) (Tg) and their nontransgenic littermates (non). C, E. Intraperitoneal (IP) glucose tolerance test (1.5 g/kg) in RIP-G Tg (C) and RGP-G Tg (E) (Tg) and their nontransgenic littermates (non). D, F: Plasma insulin concentration after IP glucose

(3g/kg) injection in RIP-G Tg (D) and RGP-G Tg (F) (Tg) and their nontransgenic littermates (non). G: Plasma insulin concentration after IP arginine (0.25g/kg) injection in RIP-G Tg (Tg) and their nontransgenic littermates (non). (H) Insulin (2.0 U/ kg) tolerance test in RIP-G Tg (Tg) and their nontransgenic littermates (non). Values are represented as mean ± SE. *: $P<0.05$ compared to nontransgenic littermates.

Fig.5 Islet morphology and β cell area in RIP-G Tg (A, B, C, D) and RGP-G Tg (E, F, G, H). The sections were stained with anti-insulin (A, E), anti-glucagon (B, F), anti-somatostatin (C, G) and anti-PP antiserum (D, H). I, J: The ratio of β cell area to that of whole section in RIP-G Tg (I) and RGP-G Tg (J). non, nontransgenic littermates; Tg, RIP-G Tg; NS, not significant.

Fig. 6 mRNA level and peptide content of insulin in RIP-G Tg (Tg) and their nontransgenic littermates (non) pancreas. A. Representative blot of Northern blot analysis of insulin. B. Insulin mRNA levels C. Insulin peptide contents. NS, not significant.

Fig. 7 A, B: Immunoreactivity of Glut-2 in the islet of RIP-G Tg (A) and nontransgenic littermates (B). C, D: Immunoreactivity of PDX-1 in the islet of RIP-G Tg (C) and nontransgenic littermates (D).

Fig. 8 mRNA level of GHS-R determined by quantitative RT-PCR in pancreas (A) and pituitary (B) of RIP-G Tg (Tg) and their nontransgenic littermates (non). NS, not significant.

Fig. 9 Batch incubation study of isolated islets of RIP-G Tg (Tg) and their nontransgenic littermates (non).

Figure 1

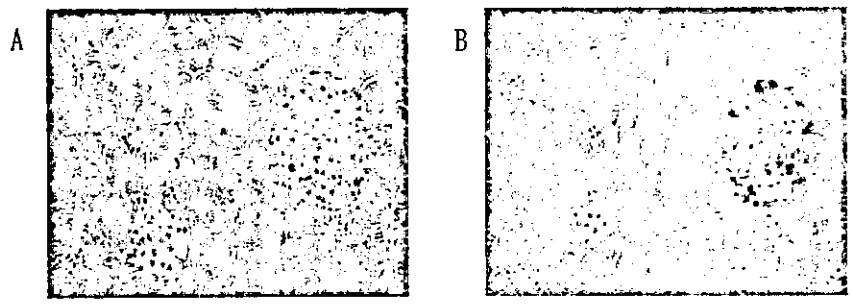

42

Figure 2

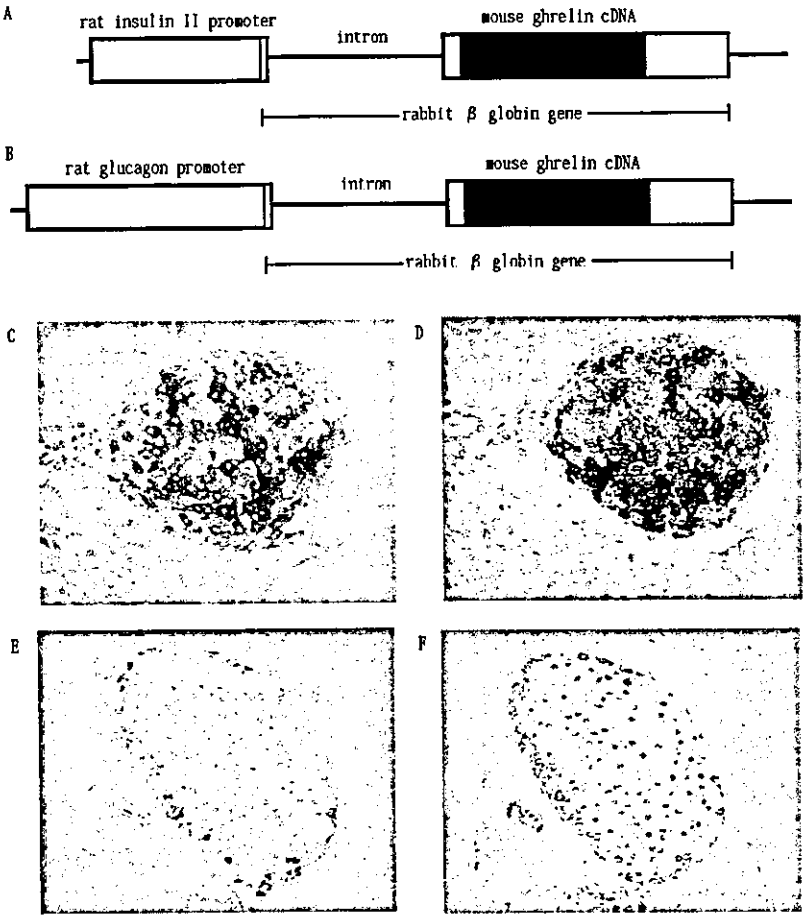
A
rat insulin II promoter
intron
mouse ghrelin cDNA
rabbit β globin gene
B
rat glucagon promoter
intron
mouse ghrelin cDNA
rabbit β globin gene
C
D
E
F

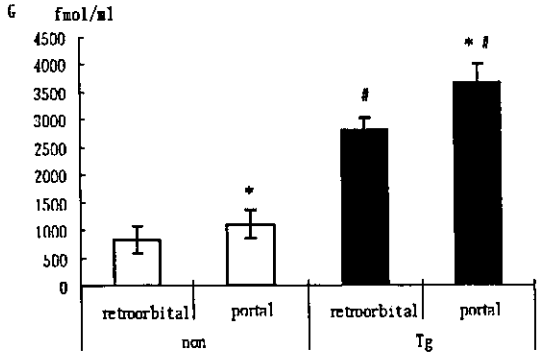
G
fmol/ml
4500
4000
3500
3000
2500
2000
1500
1000
500
0
retroorbital
portal
retroorbital
portal
non
Tg

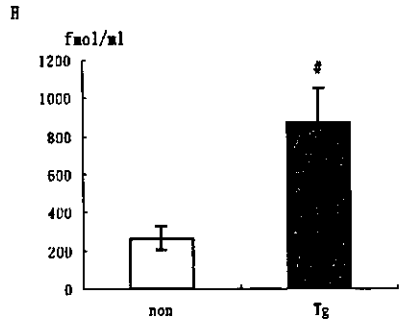
H
fmol/ml
1200
1000
800
600
400
200
0
non
Tg

43

Figure 3

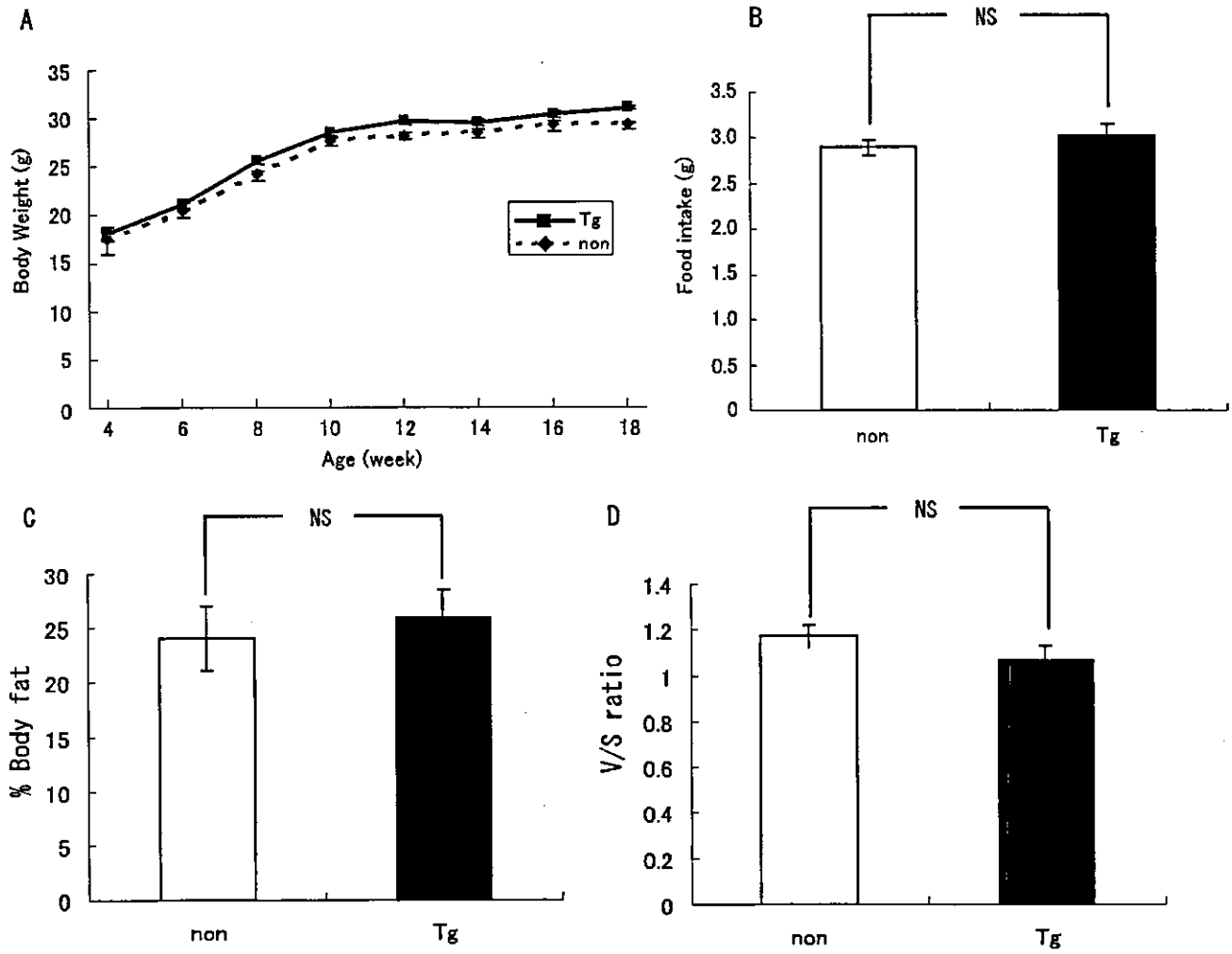
A
Body Weight (g)
35
30
25
20
15
10
5
0
4
6
8
10
12
14
16
18
Age (week)
Tg
non
B
NS
Food intake (g)
3.5
3.0
2.5
2.0
1.5
1.0
0.5
0
non
Tg
C
NS
% Body fat
30
25
20
15
10
5
0
non
Tg
D
NS
V/S ratio
1.4
1.2
1
0.8
0.6
0.4
0.2
0
non
Tg

44

Figure 4

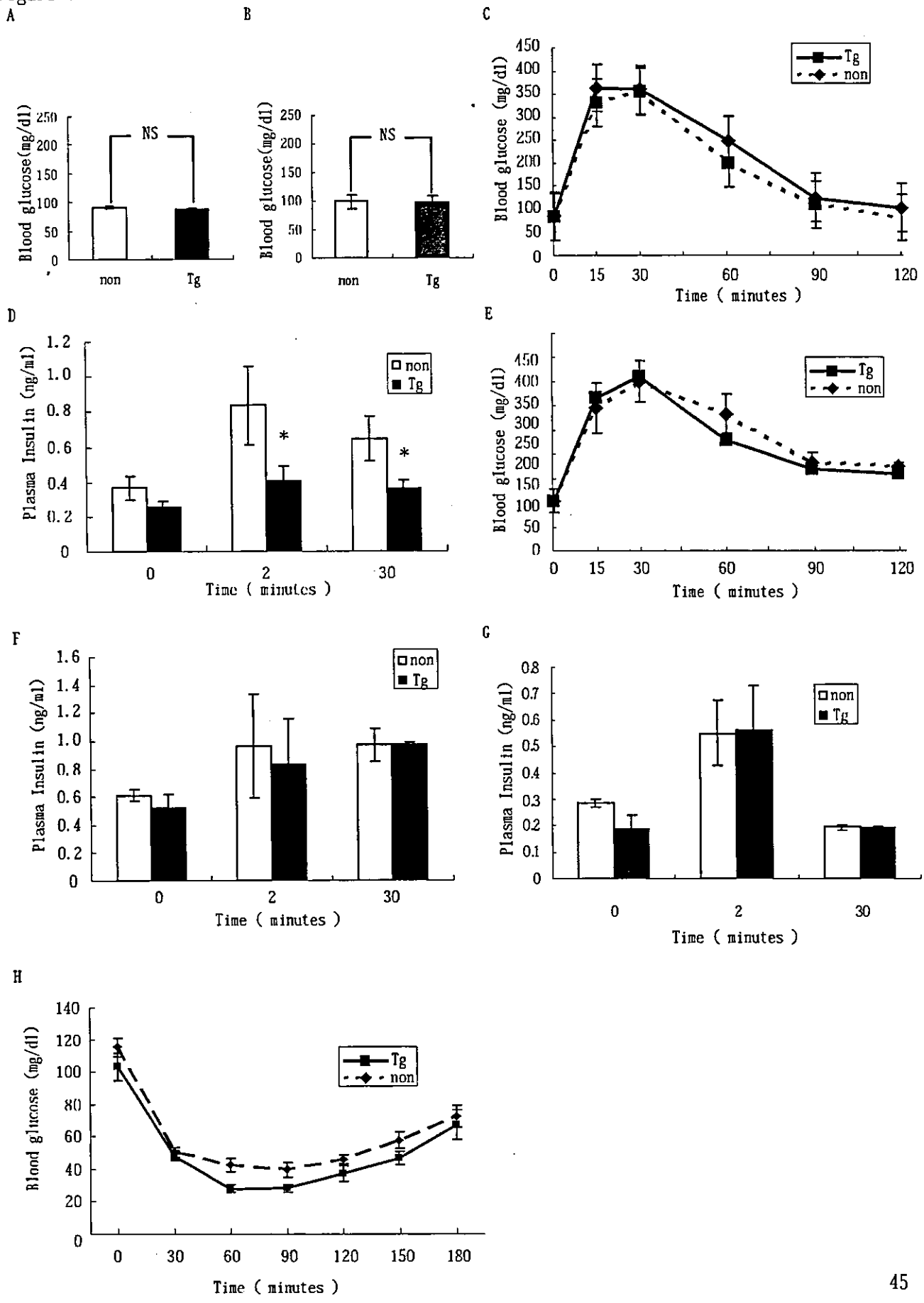
A
B
C
Blood glucose(mg/dl)
NS
non
Tg
Blood glucose (mg/dl)
Time (minutes)
D
E
Plasma Insulin (ng/ml)
*
F
G
H

45

Figure 5

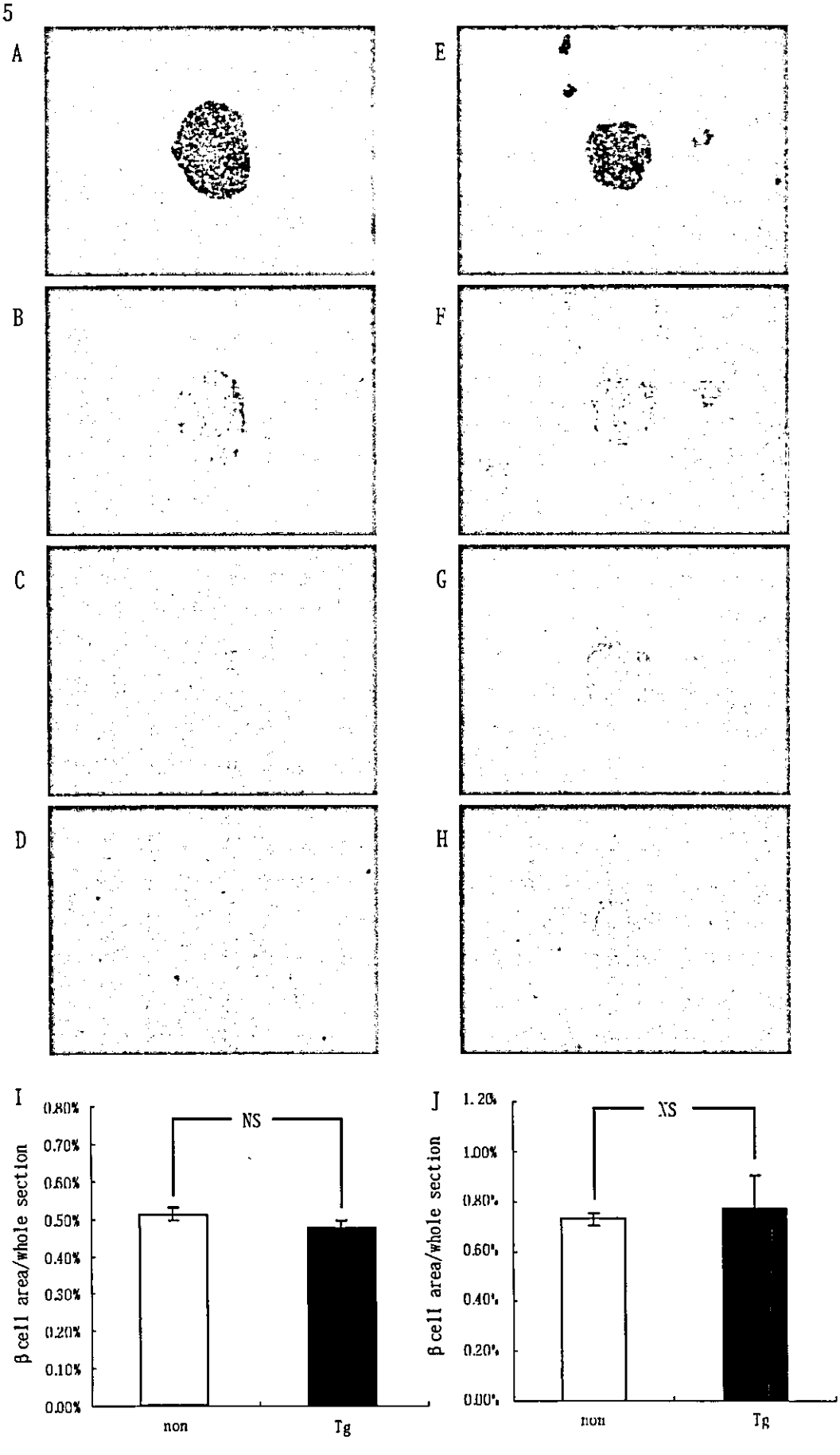
A
E
B
F
C
G
D
H
I
β cell area/whole section
0.80%
0.70%
0.60%
0.50%
0.40%
0.30%
0.20%
0.10%
0.00%
NS
non
Tg
J
β cell area/whole section
1.20%
1.00%
0.80%
0.60%
0.40%
0.20%
0.00%
NS
non
Tg

46

Figure 6

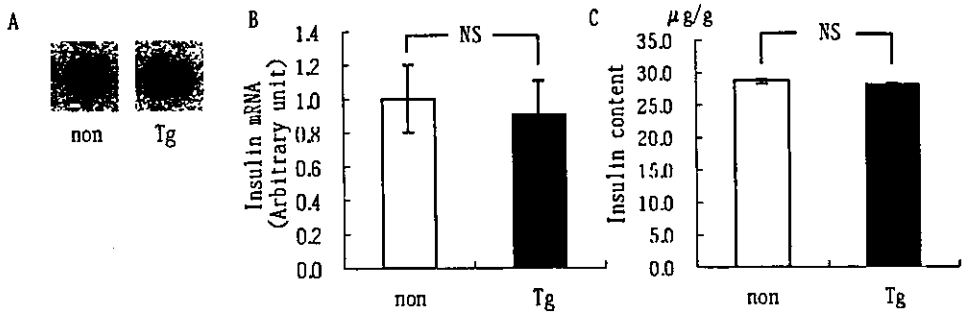
A
non
Tg
B
Insulin mRNA (Arbitrary unit)
1.4
1.2
1.0
0.8
0.6
0.4
0.2
0.0
NS
non
Tg
C
μg/g
Insulin content
35.0
30.0
25.0
20.0
15.0
10.0
5.0
0.0
NS
non
Tg

47

Figure 7

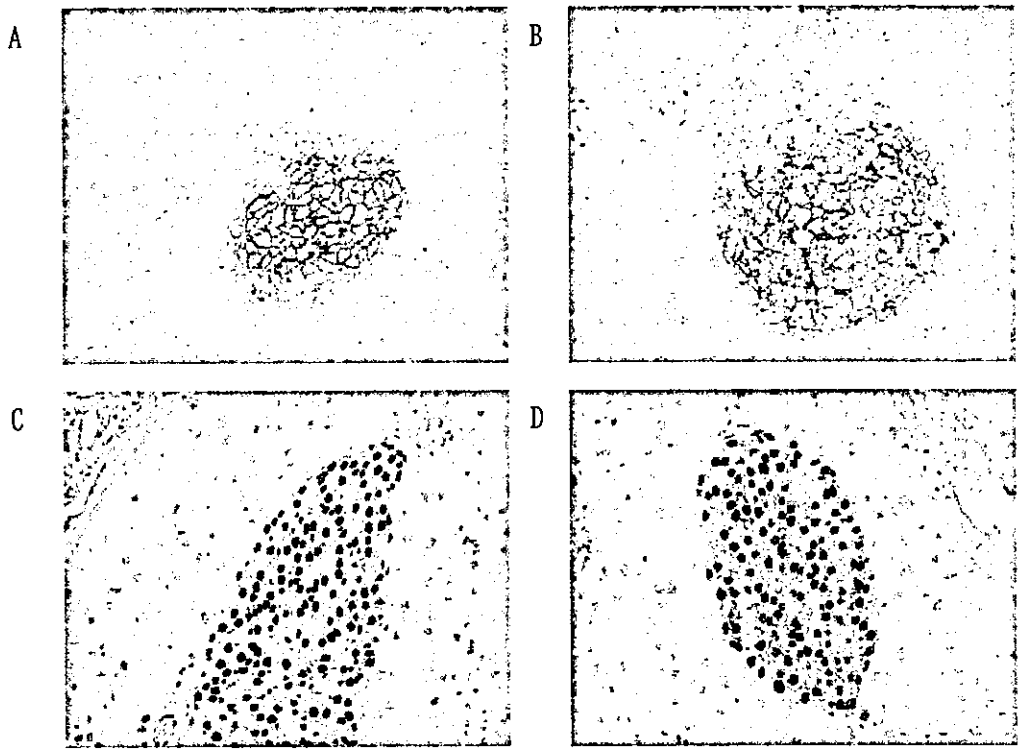

48

Figure 8

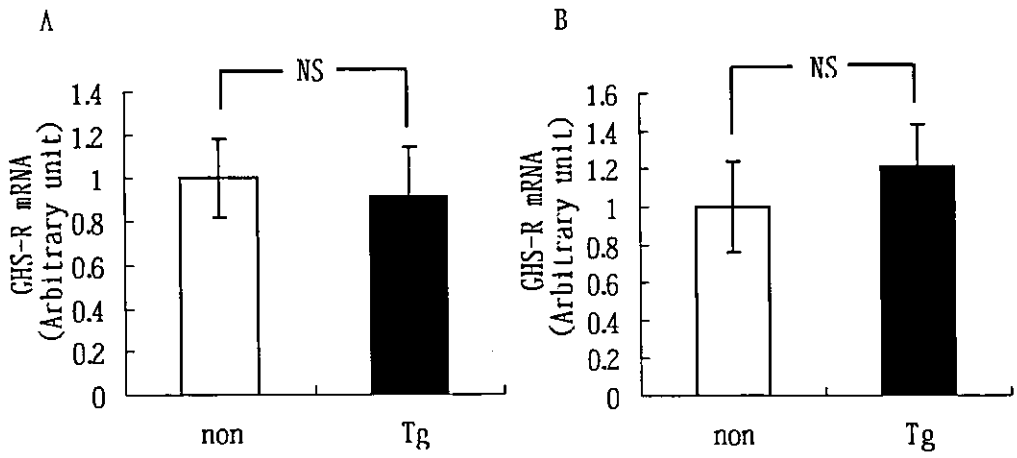

Figure 9

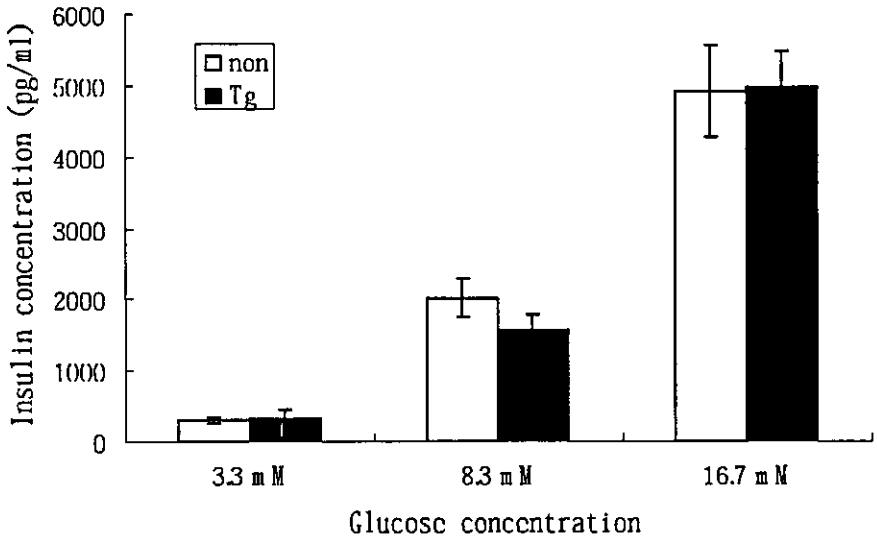
Insulin concentration (pg/ml)
6000
5000
4000
3000
2000
1000
0
non
Tg
3.3 mM
8.3 mM
16.7 mM
Glucose concentration

50

International Journal of Urology (2003) **10**, 544–546

Case Report

Successful treatment of primary aldosteronism due to computed tomography-negative microadenoma

KOJI NISHIZAWA,[1] EIJIRO NAKAMURA,[1] TAKASHI KOBAYASHI,[1] TOSHIYUKI KAMOTO,[1] AKITO TERAI,[1] TOSHIRO TERACHI,[1] OSAMU OGAWA,[1] HIROSHI ITOH[2] AND KAZUWA NAKAO[2]

Departments of [1]Urology and [2]Medicine and Clinical Science, Graduate School of Medicine, Kyoto University, Kyoto, Japan

Abstract We report a case of aldosterone-producing microadenoma that was correctly diagnosed and thus treated less invasively by laparoscopic adrenalectomy. A 58-year-old woman presented with palpitation and muscular weakness. She exhibited hypertension, hypokalemia and increased aldosterone excretion with suppressed renin activity. Therefore, primary aldosteronism was suggested. Although adrenal scintigram and computed tomography findings in the adrenal glands were normal, adrenal venous sampling tests indicated an overproduction of aldosterone in the right adrenal gland. We diagnosed an aldosterone-producing microadenoma in the right adrenal gland and performed an adrenalectomy. The patient became normotensive postoperatively and histopathological examination demonstrated a microadenoma, 5 mm in diameter.

Key words laparoscopic adrenalectomy, microadenoma, primary aldosteronism.

Introduction

Primary aldosteronism (PA) encompasses disorders characterized by hypertension, hypokalemia and increased aldosterone excretion with suppressed renin activity.[1,2] It is important to distinguish aldosterone-producing adenoma (APA) from idiopathic hyperaldosteronism (IHA) because patients with APA can be successfully managed by surgical treatment alone. However, some cases of APAs, particularly those caused by a microadenoma, are overlooked because this kind of adenoma is difficult to detect by imaging studies such as computed tomography (CT). We report a case of APA caused by a microadenoma that was correctly diagnosed and thus, treated less invasively by laparoscopic adrenalectomy.

Correspondence: Osamu Ogawa MD, Professor and Chairman, Department of Urology, Graduate School of Medicine, Kyoto University, Shogoin Kawahara-cho 54, Sakyo-ku, Kyoto City 606-8507, Japan.
Email: ogawao@kuhp.kyoto-u.ac.jp
Received 9 May 2002; accepted 24 March 2003.

Case report

A 58-year-old woman consulted our hospital with complaints of palpitation and muscular weakness. At her initial presentation, hypertension and hypokalemia were apparent. Plasma aldosterone concentration was examined and found to be 225 pg/mL (normal range, 30–160 pg/mL). No abnormal findings, such as 17-OHCS or 17-KS in urine, were observed in any of the other laboratory examinations. Thus, the patient was examined by an adrenal scintigram using ^{131}iodine adosterol and 3-mm-thick CT sections to detect aldosterone-producing adenomas (Fig. 1). However, these examinations did not detect any abnormal findings in the adrenal glands. To further examine the causes of PA, adrenal venous sampling tests with adrenocorticotropic hormone (ACTH) stimulation were performed.[3] The aldosterone concentration from the catheterized left adrenal vein was 291 and the calculation of an aldosterone/cortisol (A/C) ratio was 4.9 (below 5, in the normal range). After stimulation, the aldosterone concentration from the right and left adrenal veins increased from 1195 to 5 4198 and 291 to 1475 ng/dL, and the A/C ratios from 10 to 149 and 4.9 to 13.2, respectively. The

Fig. 1 Enhanced computed tomography of a 58-year-old woman with aldosterone-producing microadenoma shows no mass in either adrenal gland (arrows).

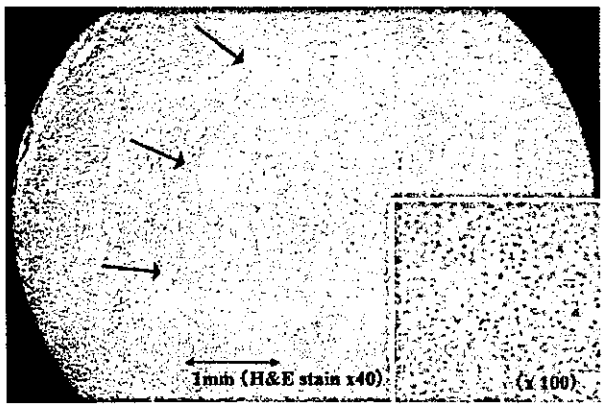

Fig. 2 Histopathological findings: solitary adenoma consisting mainly of clear cells and a small number of compact cells (H&E × 40).

overproduction of aldosterone in the right adrenal gland was highly suggestive of an aldosterone-producing microadenoma in the right adrenal gland.

After spironolactone intake alone, the patient's blood pressure decreased from 160/100 to 135/86 mmhg, and her symptoms were relieved. This was predictive of a favorable outcome by surgical management.[4] Therefore, transperitoneal laparoscopic right adrenalectomy was performed following operative procedures described previously.[5] The operation lasted for 183 min and there was little blood loss. The patient started to walk and eat on the first postoperative day. Histopathological examination indeed exhibited a microadenoma 5 mm in diameter, consisting mainly of clear cells and partly of compact cells with microscopic findings compatible with APA. The adenoma was composed of cells resembling zona glomerulosa or the hybrid type of cell. The zona fasciculata of the attached cortex showed hyperplasia and was diffusely widened (Fig. 2). After adrenalectomy, serum aldosterone level decreased from 225 to 48 pg/mL and blood pressure settled at 132/72 mmhg without spironolactone. Serum potassium concentration increased from 3.1 to 3.6 mEp/mL. Thus, plasma aldosterone levels, serum potassium and blood pressure normalized postoperatively.

Discussion

From a therapeutic point of view, an accurate diagnosis of the causes of PA is important because surgical management is a successful treatment for most patients with APA.[4] An adenoma that cannot be proved by thin-section CT, but can be proved by clinical and pathological findings is defined as a microadenoma. These adenomas are usually smaller than 1 cm in diameter, and their lateralization can be proved by venous sampling with or without stimulation.[1,3] Generally an adenoma exists in the adrenal cortex with a tenuous capsule, and its cut surface is characteristically bright yellow.[4] Recent advances in CT scanning make it possible to detect up to 90% of adenomas that cause APA.[6] Magnetic resonance imaging (MRI) may be more accurate at localizing small adenomas than CT.[7,8] Thus, it is possible that the adenoma described herein, which was up to 5 mm in diameter, might have been described on MRI.

Because adenomas smaller than 1 cm in diameter are easily missed, adrenal venous sampling tests are inevitable in some patients.[1,2,4] Indeed, many patients exhibited excessive secretion of aldosterone in this sampling, irrespective of prior normal adrenal gland findings on CT imagings.[9] A unilateral excess of aldosterone does not always indicate the presence of an aldosterone producing adenoma because the possibility of adrenal hyperplasia remains. However, unilateral adrenalectomy is usually performed because it will also improve hypertension, even in the latter case.[2,3] After adrenalectomy, a diagnosis of APA can be confirmed by histopathological analysis, changes in serum aldosterone levels and potassium, and blood pressure. In histopathological analysis, it is known that immunohistochemical study, especially for 3-beta-hydroxysteroid dehydrogenase, is helpful for making a deferential diagnosis between an aldosterone-producing adenoma and idiopathic hyperaldosteronism.[10]

Evidence is accumulating that aldosteron-producing microadenomas are present in most patients diagnosed with PA and that the prevalence of this disease among hypertensive disorders[4] could be higher than

expected.[2,9] Nishikawa and Omura diagnosed 55 cases of PA (5.4%) by adrenal venous sampling tests from 1020 patients initially diagnosed with essential hypertension.[9] Among these 55 patients, aldosteron-producing microadenomas caused PA in as many as 26 cases (47%). These results allow for the possibility that surgical management alone could cure a significant proportion of hypertensive patients if correctly diagnosed. Thus, the accurate diagnosis of aldosteron-producing microadenomas followed by laparoscopic adrenalectomy has considerable potential in the treatment of hypertensive diseases.

References

1 Sheaves R, Goldin J, Reznek RH *et al.* Relative value of computed tomography scanning and venous sampling in establishing the cause of primary hyperaldosteronism. *Eur. J. Endocrinol.* 1996; **134**: 308–13.

2 Young WF, Stanson AW, Grant CS, Thompson GB, van Heerden JA. Primary aldosteronism: adrenal venous sampling. *Surgery* 1996; **120**: 913–20.

3 Doppman JL, Gill JR, Miller DL *et al.* Distinction between hyperaldosteronism due to bilateral hyperplasia and unilateral aldosteronoma: reliability of CT. *Radiology* 1992; **184**: 677–82.

4 Ganguly A. Primary aldosteronism. *N. Engl. J. Med.* 1998; **339**: 1828–34.

5 Terachi T, Matsuda T, Terai A *et al.* Transperitoneal laparoscopic adrenalectomy: experience in 100 patients. *J. Endourol.* 1997; **11**: 361–5.

6 Radin DR, Manoogian C, Nadler JL. Diagnosis of primary hyperaldosteronism: importance of correlating CT findings with endocrinologic studies. *AJR Am. J. Roentgenol.* 1992; **158**: 553–7.

7 Nishikawa T, Omura M. Clinical characteristics of primary aldosteronism: its prevalence and comparative studies on various causes of primary aldosteronism in Yokohama Rosai Hospital. *Biomed. Pharmacother.* 2000; **54**: 83–5.

8 Rossi GP, Chiesura-Corona M, Tregnaghi A *et al.* Imaging of aldosterone-secreting adenomas: a prospective comparison of computed tomography and magnetic resonance imaging in 27 patients with suspected primary aldosteronism. *J. Hum. Hypertens.* 1993; **7**: 357–63.

9 Nakao Y, Abe I, Kobayashi K *et al.* Evaluation of the localizing procedures of primary aldosteronism. *Nippon Jinzo Gakkai Shi.* 1993; **35**: 281–6.

10 Omura M, Kagami S, Seki N *et al.* Case of primary aldosteronism caused by adrenal microadenoma that permitted clinical observation from onset. *Nippon Naika Gakkai Zasshi* 1999; **88**: 2474–5.

Cell Transplantation, Vol. 13, pp. 439–449, 2004
Printed in the USA.

0963-6897/04 $20.00 + .00

In Vivo Tissue-Engineered Small-Caliber Arterial Graft Prosthesis Consisting of Autologous Tissue (Biotube)

Yasuhide Nakayama,* Hatsue Ishibashi-Ueda,† and Keiichi Takamizawa*

*Department of Bioengineering, National Cardiovascular Center Research Institute, Fujishiro-dai 5-7-1, Suita, Osaka 565-8565, Japan
†Department of Pathology, National Cardiovascular Center Hospital, Fujishiro-dai 5-7-1, Suita, Osaka 565-8565, Japan

In this study, vascular-like tubular tissues called biotubes, consisting of autologous tissues, were prepared using in vivo tissue engineering. Their mechanical properties were evaluated for application as a small-caliber artificial vascular prosthesis. The biotubes were prepared by embedding six kinds of polymeric rods [poly(ethylene) (PE), poly(fluoroacetate) (PFA), poly(methyl methacrylate) (PMMA), segmented poly(urethane) (PU), poly(vinyl chloride) (PVC), and silicone (Si)] as a mold in six subcutaneous pouches in the dorsal skin of New Zealand White rabbits. For rods apart from PFA, biotubes were constructed after 1 month of implantation by encapsulation around the polymeric implants. The wall thickness of the biotubes ranged from about 50 to 200 μm depending on the implant material and were in the order PFA < PVC < PMMA < PU < PE. As for PE, PMMA, and PVC, the thickness increased after 3 months of implantation and ranged from 1.5-to 2-fold. None of the biotubes were ruptured when a hydrostatic pressure was gradually applied to their lumen up to 200 mmHg. The relationship between the intraluminal pressure and the external diameter, which was highly reproducible, showed a "J"-shaped curve similar to the native artery. The tissue mostly consisted of collagen-rich extracellular matrices and fibroblasts. Generally, the tissue was relatively firm and inelastic for Si and soft for PMMA. For PMMA, PE, and PVC the stiffness parameter (β value; one of the indexes for compliance) of the biotubes obtained was similar to those of the human coronary, femoral, and carotid arteries, respectively. Biotubes, which possess the ability for wide adjustments in their matrices, mechanics, shape, and luminal surface design, can be applied for use as small-caliber blood vessels and are an ideal implant because they avoid immunological rejection.

Key words: Biotube; Arterial graft prosthesis; Tissue engineering; Autologous transplant; Small caliber

INTRODUCTION

It is ideal to design transplantation tissues consisting solely of the patient's own cells and matrix components, including appropriate mechanical properties and shapes. In this study, we have attempted to develop a novel in vivo tissue-engineering technique for the design and preparation of vascular tissues with high patency at a chronic phase for autotransplantation using the patient's own cells and extracellular matrix components. It is known that when artificial materials are embedded in the body, fibroblasts appear around the implanted materials due to the action of the body's own biological defense system. This results in the formation of capsular tissues consisting of a collagen-rich extracellular matrix produced by the fibroblasts. The principle of our study was to utilize capsular tissues.

The encapsulation phenomenon has been well documented since the 1930s. Peirce et al. attempted to utilize capsular tissues as artificial vascular vessels (19,27). In the latter half of the 1960s, Sparks et al. investigated the clinical application of grafts consisting of a combination of capsular tissues and artificial Dacron blood vessels (8,34). In their study, a Dacron fabric graft with a silicone tube inside the graft was embedded into the subcutaneous tissue of a patient. When the patient's tissue gradually covered the Dacron graft, the silicone tube in the graft was removed to give an autotissue tube around the Dacron graft as a scaffold. The tube was used as an arterial bypass by anastomosis of both ends of the tube with an occluded native artery. However, because the luminal surface of the grafts was exposed with collagenous fibers, which promote thrombus formation, occlusion occurred within the early stage of implantation in almost all of the cases.

Recently, Campbell et al. investigated utilizing capsular tubular tissues alone for artificial blood vessels (5). After intraperitoneal indwelling of silicone rods for sev-

Address correspondence to Yasuhide Nakayama, Department of Bioengineering, National Cardiovascular Center Research Institute, 5-7-1 Fujishiro-dai, Suita, Osaka 565-8565, Japan. Tel: +81-6-6833-5012; Fax: +81-6-6872-8090; E-mail: nakayama@ri.ncvc.go.jp

eral weeks in rats, mice, rabbits, and dogs, tubular tissues that possessed a medial wall with several layers of myofibroblasts and a collagen-rich extracellular matrix covered with a single layer of mesothelial cells were obtained. By inverting the tubular tissues, an inner lining of the mesothelial cells was acquired as a nonthrombotic luminal surface. Autotransplantation of these tissues (3–5 mm) as grafts resulted in high patency for several months, suggesting the possible application of capsular tissues alone for arterial blood vessels at an early stage of implantation.

The patency rate after implantation of small-caliber artificial grafts is much lower than medium-to large-diameter artificial grafts due to thrombosis in early stage and neointimal hyperplasia in chronic stage. Among the many factors determining the patency of small-caliber artificial grafts, the compliance mismatch between the native artery and the artificial grafts has been discussed as a major detrimental factor of graft failure (1,17,18, 28,36). Indeed, it has been demonstrated that compliance matching of elastomeric segmented poly(urethane) (PU) tubes by microporing markedly inhibited intimal hyperplasia in an animal model (6).

In this study, the mechanical properties of the tissues were investigated as the first stage of utilizing tubular tissues formed by encapsulation for small-caliber arterial blood vessels. At first, various rod-form polymeric implants were embedded in subcutaneous pouches in the dorsal skin of rabbits to obtain tubular tissues, called biotubes, that were formed by encapsulation. The mechanical properties, including pressure resistance, pulse follow-ability, and compliance of the biotubes, were measured after histological analysis of their components. The designs of the matrix, including luminal surface, mechanics, and shape of the biotubes for specific transplantation sites, were also discussed.

MATERIALS AND METHODS

Preparation of Biotube

The experimental animals were nine New Zealand White rabbits, weighing 2.0–2.5 kg. The investigations were performed according to the Principles of Laboratory Animal Care (formulated by the National Society for Medical Research) and the Guide for the Care and Use of Laboratory Animals (National Institutes of Health Publication, No. 56-23, revised 1985). Anesthesia was induced by intramuscular injection of a mixture of ketamine (62.5 mg/kg) and xylazine (8.3 mg/kg). The dorsum of the rabbits was shaved and sterile prepped with iodine (Meiji Seika, Ltd., Tokyo, Japan). Six small incisions (approximately 1 cm long) were made laterally on the dorsal skin using a surgical blade. Subcutaneous pouches were made away from each incision using blunt scissors. Six kinds of polymers in the shape of rods (length: 20 mm; diameter: 3 mm) were placed inside each pouch. The polymer materials used were: low-density poly(ethylene) (PE, Yamaichi Co. Ltd., Osaka, Japan; specific gravity: 0.92 g/cm^3, tensile strength: 110 kg/cm^2, elongation: 650%), soft poly(vinyl chloride) (PVC, Yamaichi Co. Ltd.; tensile strength: 1.6 kgf/mm^2, elongation: 281%), poly(fluoroacetate) (PFA, Toho Kasei Co. Ltd.; specific gravity: 2.12 g/cm^3, tensile strength: 20.5 MPa, elongation: 244%), and silicone (Si, Tigers Polymer Co. Ltd., Osaka, Japan; specific gravity: 1.16, tensile strength: 10.8 MPa, elongation: 510%). All rods apart from poly(methyl methacrylate) (PMMA) and PU rods were fabricated by thermally end-capping of the tubes prepared by an extrusion molding method. PMMA rod was fabricated by Daisan Kako Co. Ltd. (Osaka, Japan) by an extrusion molding method of PMMA pellet (Delpet 60N, Asahi Chemical Co. Ltd., Tokyo, Japan; specific gravity: 1.19 g/cm^3, tensile strength: 72 MPa, elongation: 5%). All polymeric tubes and PMMA rod were obtained from Sanplatec Co. Ltd. (Osaka, Japan). Segmented PU rod was prepared by thinly dip-coating around the PMMA rod from a tetrahydrofuran solution of PU purchased from Nihon Miractrane Co. Ltd. (E980MNAT, Kanagawa, Japan). The coating thickness was about 50 μm. The incisions were closed with a 3.0 ethilon suture (Ethicon, Somerville, NJ).

At specific time points (1, 2, and 3 months) after insertion of the polymer rods, the rabbits were anesthetized with a mixture of ketamine (62.5 mg/kg) and xylazine (8.3 mg/kg). The dorsum of the rabbits was shaved and sterile prepped with iodine. Six small incisions (approximately 2 cm long) were made in the neighborhood of the implanted part on the dorsal skin. The encapsulated six implants, which were weakly covered with a membrane tissue in the subcutaneous layer, were harvested with surrounding tissues from the dorsum of each of rabbits using a surgical blade. The surrounding fragile membrane tissues covered on the obtained firm encapsular tissues were carefully removed by scissors. The biotubes that formed around the polymeric rods as a capsule were removed from the rod by trimming one end.

Histological Examination

The created biotubes were explanted and fixed by 10% buffered formalin solution and embedded in paraffin. Tissue sections were cut into 3–5-μm-thick pieces for routine hematoxylin and eosin for histological evaluation. Immunohistochemistry was also performed for identification of the muscular component of the biotubes. Antibodies to α-smooth muscle actin (α-SMA, DAKO, 1:100 dilution), vimentin (DAKO, 1:100 dilu-

tion), desmin (DAKO, 1:100 dilution), and RAM11 for rabbit macrophages (DAKO, 1:50 dilution) were applied to the serial sections of the tubular tissues using a labeled avidin-biotin (LAB) system (DAKO, Japan). Diaminobenzidine (DAB) was used as a reacting color. The thickness of the biotube walls was measured using a microscopic monometer.

Mechanical Properties

The luminal pressure–diameter relationship was determined using an apparatus designed by Takamizawa and Hayashi (37). One end of the biotube was cannulated to a fixed stainless steel connector for pressure loading and the other to a sliding connector, and the biotube was restored to in situ length in a bath filled with Krebs-Ringer solution held at 37°C. The biotube was gradually inflated with a pressurized Krebs-Ringer solution using a pump, recording the intraluminal pressure from 0 to around 200 mmHg at a rate of 5 mmHg/s. The luminal pressure, P, measured with a pressure transducer (N5901; Nihon Denki Sanei, Inc., Tokyo, Japan), and the external diameter at the center of the tube, D, were determined using an apparatus consisting of a video camera (C2400; Hamamatsu Photonics, Inc., Shizuoka, Japan), TV monitor, and width analyzer (C3160, Hamamatsu Photonics, Inc) and all were simultaneously recorded.

The compliance of the tube was determined by the stiffness parameter (β) as defined by Hayashi et al. (9,10), which is described according to the equation: $\ln(P/P_s) = \beta(D/D_s - 1)$, where P, P_s, D, and D_s denote luminal pressure, standard pressure (100 mmHg in this study), external diameter, and diameter at the pressure P_s, respectively. The logarithm of the normalized pressure [$\ln(P/P_s)$] was plotted against the normalized external diameter (D/D_s). The β value was determined as the approximate slope of the plot in the physiological blood pressure range from 60 to 140 mmHg.

RESULTS

Preparation of Biotubes

The six types of polymeric round rods, consisting of either PMMA, Si, PU, PE, PVC, or PFA, were used as a mold. In all nine rabbits, the polymeric rods were inserted separately into each subcutaneous pouch via a small incision on the rabbit's dorsal skin. After 1 month of embedding all rods were found to be encapsulated by a membrane tissue in the subcutaneous layer (Fig. 1A). The capsule that formed around the implants adhered weakly to the subcutaneous membrane tissue, making it easy to excise the implants with the surrounding capsulated tissue from the subcutaneous tissue (Fig. 1B). When one end of the tissue was opened the inner implants and the tubular tissues were not adhered and the inner implants could be easily removed without injuring the tissues, thereby obtaining tubular tissues (biotubes) whose walls were thin and relatively firm. The outer surface of the biotubes had a slightly rough appearance due to adhesion with the subcutaneous membrane tissue, but the luminal surfaces were extremely smooth. At 3 months of embedding, all implants were still covered with capsular tissues and were impregnated in the subcutaneous membrane tissue. Generally, the biotubes obtained after 3 months of embedding showed a firmer wall form than those obtained after 1 month of embedding.

Components of the Biotubes

Cross sections from the obtained biotubes were histologically investigated. For all biotubes the size of the inner diameter that formed around the polymeric round rods after 1 month of embedding was similar to the outer diameter of the mold, about 3 mm (Fig. 2A), and the wall thickness was almost uniform. The thickness of the biotube walls was around 70 μm after 1 month of embedding when Si, PVC, or PFA implants were used and around 100–150 μm when PU or PMMA implants were used (Figs. 3 and 4). The wall was thickest (around 200 μm) when the PE implant was used. For all implants the inner diameter did not change after 3 months of embedding compared with 1 month of embedding. However, the wall thickness increased (1.5-to 2-fold) for PMMA, PVC, and PE (Fig. 3). The structure of the biotube walls formed after 3 months of embedding is shown in Figure 4. The biotube walls that formed around the PFA rod had sparse collagen fibers and contained relatively abundant component spindle cells consistent with fibroblasts. Regarding the Si rod, the biotube wall was thin but collagen fibers with a close mesh structure were layered and almost no component cells were observed. Regarding the PMMA, PU, and PVC rods, the walls formed a moderate thickness and relatively large collagen fibers formed around the mesh structures. Fibroblasts as component cells were abundant and the biotubes that formed around the PU and PVC bases contained a number of inflammatory cells. Regarding the PE rod, the wall was very thick but almost no regular mesh structure of collagen fibers formed.

From immunohistochemical studies vimentin, a mesenchymal tissue marker, was positive for all tubular tissues around the various rods after 1 and 3 months of embedding (Fig. 5). α-SMA was intensely positive for all tubular tissues after 3 months. Desmin as a cytoskelton of matured muscle was negative in all tubular tissues after 1 and 3 months. Inflammatory cells such as lymphocytes and foreign body giant cells were observed in

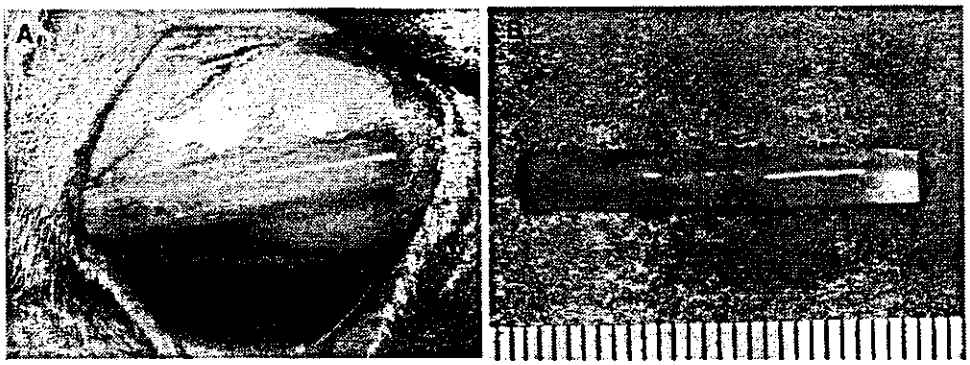

Figure 1. (A) Macroscopic observation of the biotube, impregnated in the rabbit dorsal subcutaneous tissue, which was formed by implantation of the PMMA round rod (diameter: 3 mm, length: 2 cm) for 1 month into a subcutaneous pouch prepared on rabbit dorsal skin. (B) The external view of the biotube with the PMMA rod inside extracted from the rabbit dorsal subcutaneous tissue.

the tubular tissues of PE and PU as described above. RAM11, a marker of rabbit macrophages, was observed for a small number of macrophages among the tubular tissues of PU, PFA, and PMMA after 3 months of implantation.

Mechanical Properties of the Biotubes

Changes in the outer diameter of the biotubes were measured when both ends of the biotubes were closed and a water pressure was continuously added to the lumen. None of the biotubes ruptured even after 200 mmHg inner pressure, showing pressure resistance after only 1 month of implantation (Fig. 6). The external diameter of the biotubes around the Si rod became slightly dilated when exposed to water at low pressure but did not change significantly with increased pressure (about 20 mmHg or higher) (Fig. 6). In contrast, the external diameter of the biotube that formed around the PMMA rod became dilated at low-pressure ranges and gradually increased with pressure up to a high range, indicating "J"-shaped curves (Fig. 6). The dilatation rate of the outer diameter at a water pressure of 200 mmHg was about 5% for Si and about 25% for PMMA.

Water pressure was repeatedly loaded and removed in the lumen of the biotube that formed around the PMMA rods within a range of 0 to 200 mmHg, and changes in the external diameter were investigated (Fig. 7). The external diameter of the biotube was about 2.7 mm before loading and dilated to about 3 mm after loading at several 10-mmHg water pressure and thereafter continuously dilated slowly with an increase in inner pressure load, reaching about 3.2 mm at a luminal pressure of 200 mmHg. When the water pressure was removed the outer diameter gradually decreased and

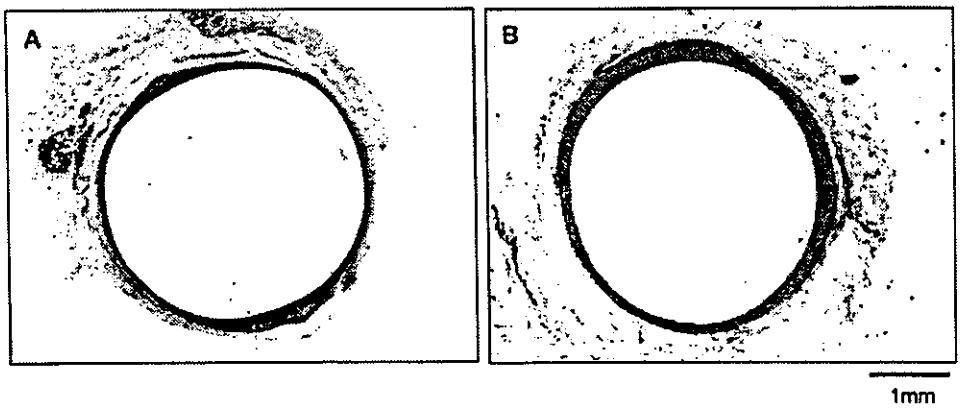

Figure 2. Circumferential sections of the biotubes formed by implantation of the PMMA round rod in the rabbit dorsal subcutaneous pouch for (A) 1 month or (B) 3 months (hematoxylin and eosin stain).

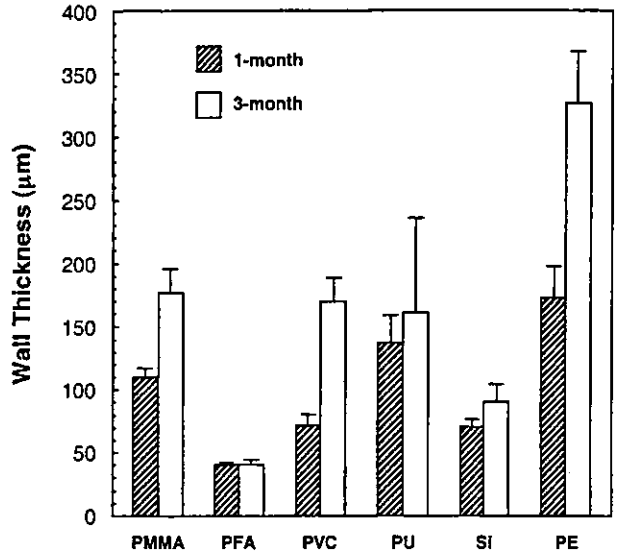

Figure 3. Implantation period-dependent changes of wall thickness of the biotubes formed around the six kinds of polymers.

reached about 3 mm at several 10 mmHg then rapidly decreased and returned to its original diameter before loading water pressure began, about 2.7 mm at 0 mmHg. Changes in the outer diameter with luminal pressure were basically the same with repeated pressure loadings in the lumen. In the case of biotubes prepared using other implants, repeat experiments produced almost identical changes.

The relationship between logarithmic value of the relative pressure and relative outer diameter was obtained from the relationship between outer diameter and luminal pressure. Because a linear relationship was obtained within a physiological range of pressure, β values were calculated from the slope of the line at a point near the standard inner pressure (100 mmHg). After 1 month of implantation, the highest β value was obtained from the biotube formed around the Si base and the β value decreased in the order of PMMA, PE, and PVC (Fig. 8). The biotube that formed around the PMMA rod exhibited a β value close to that of the human coronary artery whereas the β values of the biotubes formed around the PE and PVC bases were close to those of the human femoral and common carotid arteries, respectively. The β value of the biotube formed around the PMMA rod was about 30 after 1 month of embedding and increased linearly to about 80 after 3 months of embedding (Fig. 9).

DISCUSSION

Considering problems such as immunological rejection, it is important that tissues and organs for transplantation should consist solely of autotissues. However, it is sometimes difficult to obtain appropriate biocompatible tissues for transplantation, even for blood vessels. For example, the patient's own vessels (autografts) are used

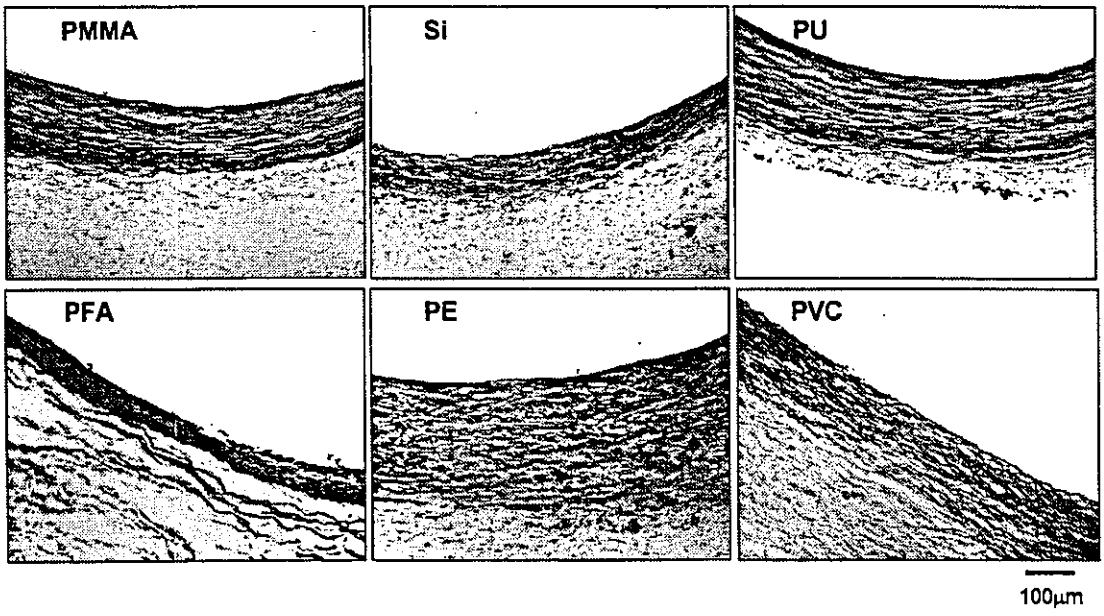

Figure 4. Circumferential sections of the biotubes formed by 3 months of implantation of six kinds of polymer round rods in the rabbit dorsal subcutaneous pouch (hematoxylin and eosin stain). Upper side of the wall of the biotube in each photo indicates luminal surface.